PUBLICATIONS OF THE ASTRONOMICAL SOCIETY OF THE PACIFIC, 111:1539–1558, 1999 December
© 1999. The Astronomical Society of the Pacific. All rights reserved. Printed in U.S.A.

Calibration of the MACHO Photometry Database

C. ALCOCK,[1,2] R. A. ALLSMAN,[3] D. R. ALVES,[1,4,5] T. S. AXELROD,[6] A. C. BECKER,[7] D. P. BENNETT,[2,5,8] K. H. COOK,[1,2,5] A. J. DRAKE,[6] K. C. FREEMAN,[6] M. GEHA,[1] K. GRIEST,[2,9] M. J. LEHNER,[10] S. L. MARSHALL,[1,5] D. MINNITI,[1,11] B. A. PETERSON,[6] P. POPOWSKI,[1] M. R. PRATT,[12] C. A. NELSON,[13] P. J. QUINN,[14] C. W. STUBBS,[2,7] W. SUTHERLAND,[2,15] A. B. TOMANEY,[7] T. VANDEHEI,[9] AND D. L. WELCH[16]

(THE MACHO COLLABORATION)

Received 1998 October 23; accepted 1999 August 30

ABSTRACT. The MACHO Project is a microlensing survey that monitors the brightnesses of ~ 60 million stars in the Large Magellanic Cloud (LMC), Small Magellanic Cloud, and Galactic bulge. Our database presently contains about 80 billion photometric measurements, a significant fraction of all astronomical photometry. We describe the calibration of MACHO two-color photometry and transformation to the standard Kron-Cousins V and R system. Calibrated MACHO photometry may be properly compared with all other observations on the Kron-Cousins standard system, enhancing the astrophysical value of these data. For ~ 9 million stars in the LMC bar, independent photometric measurements of $\sim 20{,}000$ stars with $V \lesssim 18$ mag in field-overlap regions demonstrate an internal precision $\sigma_V = 0.021$, $\sigma_R = 0.019$, $\sigma_{V-R} = 0.028$ mag. The accuracy of the zero point in this calibration is estimated to be ± 0.035 mag for stars with colors in the range -0.1 mag $< V-R < 1.2$ mag. A comparison of calibrated MACHO photometry with published photometric sequences and new *Hubble Space Telescope* observations shows agreement. The current calibration zero-point uncertainty for the remainder of the MACHO photometry database is estimated to be ± 0.10 mag in V or R and ± 0.04 mag in $V-R$. We describe the first application of calibrated MACHO data: the construction of a color-magnitude diagram used to calculate our experimental sensitivity for detecting microlensing in the LMC.

1. INTRODUCTION

The MACHO Project is a microlensing survey experiment (Alcock et al. 1997) that monitors the brightness variations of ~ 60 million stars in the Large Magellanic Cloud (LMC), Small Magellanic Cloud (SMC), and Galactic bulge. Microlensing is the rare transient magnification of a background source star due to the gravitational effect of a massive compact object crossing the line of sight. Paczyński (1986) first noted that if the dynamically inferred Galactic dark halo was composed of massive compact objects, the probability of microlensing would be $\tau \sim 5 \times 10^{-7}$ toward the LMC, within reach of dedicated observational surveys. The MACHO Project survey observations are made with a mosaic of charge-coupled devices (CCDs) imaging simulta-

[1] Lawrence Livermore National Laboratory, Livermore, CA 94550.
[2] Center for Particle Astrophysics, University of California, Berkeley, CA 94720.
[3] Supercomputing Facility, Australian National University, Canberra, ACT 0200, Australia.
[4] Department of Physics, University of California, Davis, CA 95616; now affiliated with the Space Telescope Science Institute, Baltimore, MD 21218; alves@stsci.edu.
[5] Visiting Astronomer, Cerro Tololo Inter-American Observatory, which is operated by the Association of Universities for Research in Astronomy, Inc., under cooperative agreement with the National Science Foundation.
[6] Mount Stromlo and Siding Spring Observatories, ANU, Weston Creek, ACT 2611, Australia.
[7] Departments of Astronomy and Physics, University of Washington, Seattle, WA 98195.
[8] Physics Department, University of Notre Dame, Notre Dame, IN 46556.
[9] Department of Physics, University of California, San Diego, La Jolla, CA 92093.
[10] Department of Physics, University of Sheffield, Sheffield S3 7RH, England, UK.
[11] Departmento de Astronomia, Pontificia Universidad Catolica, Casilla 104, Santiago 22, Chile.
[12] Center for Space Research, MIT, Cambridge, MA 02139.
[13] Department of Physics, University of California, Berkeley, CA 94720.
[14] European Southern Observatory, Karl-Schwarzschild-Strasse 2, D-85748, Garching, Germany.
[15] Department of Physics, University of Oxford, Oxford OX1 3RH, England, UK.
[16] Departments of Physics and Astronomy, McMaster University, Hamilton, ON L8S 4M1, Canada.

neously in nonstandard blue and red passbands. The special-purpose instrument is permanently mounted on the 50 inch Great Melbourne Telescope in Australia (Hart et al. 1996). The total sky area monitored is approximately 40, 3, and 45 deg^2 in the LMC, SMC, and Galactic bulge, respectively. Each star is represented in the MACHO database by a time series of two-color photometric measurements. In some cases, stars are counted in the database two or three times because the survey fields overlap on the sky.

In this paper, we describe the calibration of MACHO photometry data. Calibration actually encompasses several levels of detail regarding the systematic transformation of the MACHO data to a meaningful absolute system. The first level of calibration is the creation of an instrumental system. The second level of calibration is the transformation of the instrumental photometry to the Kron-Cousins V and R standard system.[17] This level of calibration allows for proper comparison of MACHO data with all other data on this system. In practice, these two levels of calibration are not implemented separately. The third level of calibration discussed in this paper is the calibration of light curves, i.e., analysis-stage corrections that may be applied to time series photometric data for individual stars. These corrections will eliminate some systematic sources of scatter in the photometry. Our first effort is to calibrate the "top 22" LMC fields analyzed in Alcock et al. (1997).

The MACHO Project microlensing analyses involve the photometric calibration in a number of ways. First, regions of the LMC color-magnitude diagram (CMD) excluded in the search for microlensing because of the high background of intrinsic variable stars are more accurately defined with the calibrated data. It is also possible to make a more precise comparison of the distribution of microlensing source stars in the CMD with that expected for true microlensing. Finally, calibration plays an important role in the analysis of LMC microlensing through the calculation of our experimental sensitivity to detect microlensing, which we call the "efficiency."

The microlensing efficiency calculation requires a critical assumption regarding the true distribution of stars in the LMC for the following reason. Individual stars in the ground-based MACHO image data are almost always confused, i.e., they are composites of two or more unresolved companions. However, only one true LMC star will be lensed. The partial magnification of flux from an unresolved, composite star is an effect known as "blending" in microlensing. Observational data and further discussion of blending can be found in Alcock et al. (1997). It is useful to distinguish an apparent star in the MACHO data which is actually a blend of several real "stars" by referring to it as an "object." The efficiency calculation (an exhaustive series of artificial star tests and Monte Carlo experiments) returns our experimental sensitivity to detect microlensing of stars, not objects.

In order to quantify the ratio of stars to objects, we have obtained *Hubble Space Telescope* (*HST*) imaging data in their filter equivalents of V and R for three fields in the LMC top 22. The high spatial resolution of the *HST* allows us to probe to fainter magnitudes than possible with our ground-based data, particularly in the crowded bar region. The *HST* and MACHO data are properly comparable after their respective calibration to the Kron-Cousins standard V and R magnitude system. We construct the "efficiency CMD," which is a properly scaled splicing of MACHO and *HST* data together into a CMD that also contains accurate information on the numbers of stars. The scaling factor is essentially the sought-after star-to-object ratio. The efficiency CMD described here has been used to seed millions of artificial stars into our raw image data and is the first application of calibrated MACHO data. Complete discussions of the new LMC microlensing analysis, the efficiency calculation, and the *HST* data reduction are beyond the scope of this paper; each will be the subject of a forthcoming paper.

In addition to microlensing, the MACHO photometry database is a valuable resource for studying the stellar populations and star formation history of the LMC, making new tests of stellar evolution theory, and studying variable stars. Calibration enhances the value of the MACHO database for these so-called science by-products. For this reason, *we give special attention to details of the calibration that may be relevant to consumers of released MACHO data.*

Our paper is organized as follows. In § 2, we preface the calibration discussion with some details of the MACHO image and photometry data. In § 3, we review the calibration of the LMC top 22 fields. In § 4, we compare the calibrated MACHO data with a sample of published photometric sequences in the LMC and with the new *HST* observations. In § 5, we describe the status of calibration for the remaining fields in the LMC, SMC, and Galactic bulge. In § 6, we review the calibration of MACHO instrumental light curves. In § 7, we examine the *HST* and MACHO data in greater detail and construct the efficiency CMD. Finally, in § 8 we summarize our results.

2. MACHO DATA

2.1. Images

The MACHO experiment has dedicated use of the 1.27 m (50 inch) Great Melbourne Telescope (Robinson & Grubb 1869), now located at the Mount Stromlo Observatory in

[17] For an excellent discussion of different optical broadband photometric systems, the reader is referred to Bessell (1979, 1986, 1990, 1995 and Bessell & Weis (1987)).

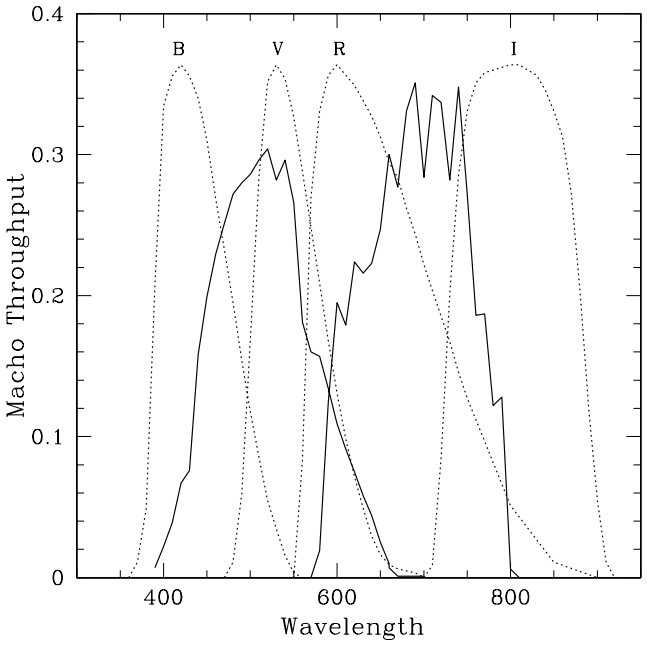


FIG. 1.—Approximate instrumental throughput for the blue and red MACHO image data. A throughput of one would indicate no loss of light; wavelength is in units of nm. These response functions include the dichroic, filters, and CCDs. However, the wide-field optics corrector has not been included. Uncertainty in these functions is ~20%. Also shown are normalized standard passbands *B*, *V*, *R*, and *I*.

Australia. A system of corrective optics has been installed at the prime focus, giving a focal reduction to f/3.9 and a 1° field of view. A dichroic beam splitter enables simultaneous blue and red imaging (Hart et al. 1996). Observations may be made from either side of the telescope pier (a German equatorial mount), i.e., either an east or west of pier observation. The median stellar image FWHM is 2″. The typical sky for an LMC bar field is estimated to be $R \sim 19.5$ mag arcsec^{-2}.[18]

The MACHO filters were specially designed to provide an adequate color index and wide bandpasses. The blue filter runs from ~4500 to 6300 Å and the red filter runs from ~6300 to 7600 Å. At both the red and blue foci, a mosaic of four 2048 × 2048 Loral CCDs are mounted. In Figure 1, we show the approximate response of the dichroic, filters, and CCDs. The wide-field optics corrector has not been included. Uncertainty is estimated to be ~20% in these response functions. The normalized standard *BVRI* passbands from Bessell (1990) are also shown.

The Loral CCD pixel size is 15 μm which corresponds to 0.″635 on the sky, giving a sky coverage of 0.52 deg^2 per MACHO field. Each CCD has two readout amplifiers, and the images are read out through a 16 channel system and written into dual-ported memory in the data acquisition computer. The readout time is 67 s per image, and the noise is ~10 e^- rms, with a gain of ~2 e^- ADU^{-1}. Further details of the MACHO camera system are provided in Stubbs et al. (1993) and Marshall (1994).

In Figure 2, we present a schematic drawing of the red and blue MACHO focal planes from both the east and west sides of the pier. We label each CCD (0–3 on the red side, and 4–7 on the blue side) and each amplifier (0.0 or 0.1). The CCD-amplifier designated 0.0 is inoperative; it is marked with an "X." For the purposes of photometry, each red and blue MACHO image is divided into 64 "chunks" (128 total), each approximately 512 × 512 pixels in size. Chunks are defined as regions of a certain CCD and amplifier in the MACHO focal plane.[19] Every red chunk uniquely corresponds to a blue chunk. In the bottom two panels of Figure 2, we present chunk maps in the west of pier orientation.

2.2. SoDOPHOT

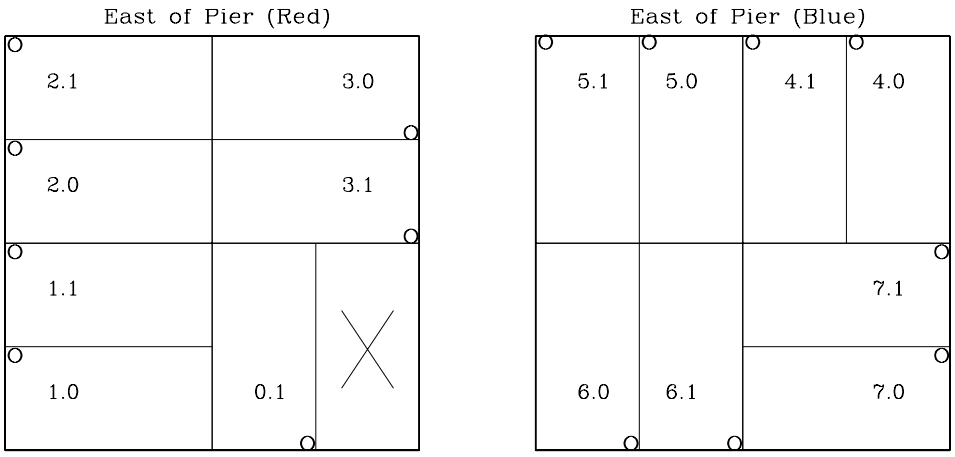
The photometry for the MACHO experiment is handled by a special-purpose code called SoDOPHOT, which stands for "Son of DOPHOT." The reader is referred to Schecter, Mateo, & Saha (1993) for further details of DOPHOT. Briefly, it is a model-based fitting code that searches for objects in two-dimensional digital array images of the sky. Stars, galaxies, cosmic rays, and so forth are each assigned a specific model defined in terms of analytic functions. Objects are identified and photometered with precise signal-to-noise criteria based on the model fits. DOPHOT may tend to report brighter magnitudes for faint stars in crowded regions than DAOPHOT (Stetson 1987), a similar type of photometry code that is widely employed by astronomers. This systematic effect is attributed to the sky fitting procedure (Schecter et al. 1993) and is likely preserved in SoDOPHOT.

SoDOPHOT is basically DOPHOT optimized to the MACHO image data and modified for extremely fast CPU reduction times. Most of the improvement in speed can be attributed to the fact that we observe the same fields repeatedly. We designate a high-quality image of a given field as a "template" image and use the reduction of our template image to help with the reduction of the other images. The template star lists are generated by an iterative and automated DOPHOT reduction which employs both the red and blue MACHO template images.

For routine reductions, SoDOPHOT makes a list of stellar positions and brightnesses of the brightest stars in

[18] This estimate likely includes some contribution from an unresolved stellar background in the LMC bar. It is calculated from ~200 images of one field spanning the full range of conditions encountered over 4 years of observations.

[19] Template photometry for certain chunks may be derived from a different CCD-amplifier image than its otherwise "defined" location in the focal plane.



West of Pier (Red)

124	120	4	0	15	14	13	12
125	121	5	1	11	10	9	8
126	122	6	2	23	22	21	20
127	123	7	3	19	18	17	16
48	49	50	51	31	30	29	28
52	53	54	55	27	26	25	24
40	41	42	43	39	38	37	36
44	45	46	47	35	34	33	32

West of Pier (Blue)

108	109	110	111	96	100	88	92
104	105	106	107	97	101	89	93
116	117	118	119	98	102	90	94
112	113	114	115	99	103	91	95
63	59	71	67	79	75	87	83
62	58	70	66	78	74	86	82
61	57	69	65	77	73	85	81
60	56	68	64	76	72	84	80

FIG. 2.—Schematic of the MACHO focal plane (red, *left*; blue, *right*) in the east of pier (*top*) and west of pier (*middle*) orientation. CCD-amplifier combinations are labeled. The inoperational amplifier 0.0 is marked with an "X." The bottom two panels are the chunk maps of the red (*left*) and blue (*right*) MACHO focal planes in the west of pier orientation. Chunks are always fixed to the same CCD-amplifier. Thus, the chunk map rotates 180° when in the east of pier orientation.

the new image and finds a crude transformation to the positions and relative brightness of stars from the template. This transformation is then used to find the approximate location of a set of about 40 bright and relatively isolated fiducial stars per chunk which have been preselected from the list of template stars. SoDOPHOT reductions are done on individual chunks, i.e., $\sim 1/16$ of a Loral CCD and $\sim 1/64$ of the imaged area in the focal plane. The fiducial stars are then subject to a seven-parameter fit to find their precise position, brightness, and point-spread function (PSF) shape. The PSF model is a three-parameter "pseudoelliptical" Gaussian and the remaining parameter to be fitted is the sky background. SoDOPHOT never attempts a fit with the galaxy model PSF that may be familiar to users of DOPHOT.

The PSF fit parameters from the fiducial stars are averaged to determine a PSF model for the new image and the fit magnitudes are averaged (after removing "outliers," i.e., variable stars) to find the magnitude offset for the new image. The fit positions of the fiducials are used to determine an accurate transformation between the template and image coordinates using a general linear transformation. With the new coordinate transformation, a magnitude offset from the template, and a new PSF, we have enough information to construct a model of all the stars in the new image. The next step is to subtract these model images and then search the subtracted image for high pixels which are subject to a cosmic-ray test. After the pixels determined to be cosmic rays are removed from the reduction, the coordinate transformation, PSF, and magnitude offset parameters are refined with a new fit of the fiducial stars.

Next, the entire star list is run through (in order of template brightness and with the stellar positions fixed) with each star being added back to the subtracted image and subject to a two-parameter fit to determine its magnitude and sky background. SoDOPHOT will simultaneously fit pairs of stars if they are adjacent (known as "splits"), but no more than two stars at once. This is the step that generates the photometry for the vast majority of the stars. After this, there are two more steps designed to improve the photometry in regions where a significant variation is detected. First, the subtracted image is searched for high pixel values, and the high pixels are determined to be either noise spikes, cosmic rays, or new stars. This procedure ensures that any moderately bright new stars in the image will be detected. Finally, stars which showed a significant variation from their template magnitudes and their neighbor are subjected to an additional round or two of fitting. This reduces the possibility that some of the flux from the variation of one star will end up being associated with a close neighbor instead.

Only stars detected in the templates are included in the MACHO database. Routine SoDOPHOT reductions are then passed through a filter to search for new microlensing events in real time. We refer to microlensing events detected in real time as "alert events." Alert events may be monitored by follow-up networks searching for exotic microlensing phenomena. A separate database of new objects detected during routine SoDOPHOT reductions is also maintained (the SodAlert files). These files are immediately compressed and exported to a mass store device; they are not analyzed.

A SoDOPHOT instrumental magnitude is the 2.5 times the base-10 logarithm of the integrated number of electrons in the fit to the analytical PSF, divided by 100. No aperture correction is calculated. SoDOPHOT keeps track of the quality of its photometry with an integer flag (i-type), which is returned for every measurement. In Table 1, we summarize the different integer flags and their meanings. SoDOPHOT photometric measurements flagged as "unconverged" or "obliterated" are generally regarded with caution. These data flags (and others) are found in the full database and are not necessarily public. Table 1 illustrates one set of data flags that may be used for quality control on released MACHO data.

2.3. Templates

Images acquired during the first few months of the experiment were selected for good seeing and low sky brightness to create one-time master star lists for each field. The most important criteria for selecting template images were the

TABLE 1

SoDOPHOT Integer Flags[a]

i-type[b]	Meaning
1	Bright, unsplit star
2	Bright, split star
3	Faint, unsplit star
4	Faint, split star
5	Very faint or unconverged unsplit star
6	Very faint or unconverged split star
7	Too faint or off the image, unsplit star
8	Too faint or off the image, split star
9	Unconverged in seven-parameter fit
10	Large number of pixels missing (>35%)
11	Cosmic ray
12	Galaxy (currently disabled)
13	Obliterated star

[a] These data flags (and others) are found in the full MACHO database and are not necessarily public. This table lists one set of data flags that may be used for quality control on released MACHO data.

[b] The i-type is modified by a boundary flag: i-type = i-type(as above) + 20(template boundary flag) + 40(boundary flag). The (template boundary flag) = 1 for stars within 10 pixels of a template chunk boundary and 0 otherwise. The (boundary flag) = 1 for stars within 10 pixels of a routine reduction chunk boundary, 2 for stars which fall off the image altogether, and 0 otherwise.

depth of the photometry, i.e., the limiting magnitude, and the total number of stars detected in each image. It was not necessary that the template images were obtained in photometric conditions.

Templates for LMC and SMC fields were constructed from two observations to minimize the loss of sky coverage due to the inoperative amplifier (0.0). Therefore, template photometry is derived from $\frac{3}{4}$ of an image taken from one side of the pier, and $\frac{1}{4}$ from the opposite side of pier. Templates constructed from CCDs 1, 2, and 3 (red) and 4, 5, and 6 (blue) from the west of pier and CCDs 2 (red) and 5 (blue) from the east of pier are designated "west of pier style templates." Templates constructed from $\frac{3}{4}$ of an east of pier image and $\frac{1}{4}$ west of pier image are designated "east of pier style templates." The situation is different for the MACHO bulge data where all templates are constructed from west of pier images only. Stars positioned on amplifier 0.0 in the bulge have only blue photometry. Templates for the Bulge are designated "Bulge-style templates." Bulge-style templates are most similar to west of pier style templates, except that CCDs 0 and 7 are employed.

Two copies of the template photometry are stored for use by the MACHO data reduction pipeline (Axelrod et al. 1998) for LMC and SMC observations. These two copies of the master photometry lists are for east and west of pier observations and are nearly identical. However, the blue photometry for the opposite side of pier from which the photometry was derived is *modified* to approximately account for the response of the different CCDs and for a focal-plane position-dependent color gradient (attributed to the dichroic). This effect is known as "blue jitter." The modification of the opposite-pier side blue template photometry is designated the "blue jitter correction." The template photometry without blue jitter corrections was used for the database calibration described in the following sections.

3. CALIBRATION OF THE LMC TOP 22 FIELDS

3.1. The Calibration Algorithm

It is useful to introduce the adopted calibration equations and coefficients, and then review their derivation in greater detail. The adopted transformation of MACHO instrumental photometry to Kron-Cousins V and R uses four coefficients for each passband: a zero point, a color coefficient, a color air-mass coefficient (where the air mass of the template observation is employed), and a chunk offset. Some stars do not have two-color photometry and so transformations are only approximate.[20] The transformation equations have the form

$$V = V_{M,t} + a0 + (a1 + 0.022X_t)(V_{M,t} - R_{M,t}) + \mathrm{co} + 2.5 \log (\mathrm{ET}) , \quad (1)$$

$$R = R_{M,t} + b0 + (b1 + 0.004X_t)(V_{M,t} - R_{M,t}) + \mathrm{co} + 2.5 \log (\mathrm{ET}) , \quad (2)$$

where V and R without subscripts indicate calibrated magnitudes on the Kron-Cousins system. We designate raw MACHO magnitudes with the subscript "M". The subscript "t" indicates a template magnitude. The term X_t represents air mass of the template observation. The term "co" stands for chunk offset. The standard exposure time correction is explicit in equations (1) and (2); it is 2.5 times the base-10 logarithm of the exposure time (ET) in seconds. An exposure of 300 s is used for observations of all LMC fields, 150 s for Bulge fields, and 600 s for SMC fields.

The calibration coefficients are identified as follows. The zero-point coefficients in the red and blue are $a0$ and $b0$, respectively. These coefficients are common to all stars in any of the 16 chunks on one Loral CCD in a MACHO field. The zero points implicitly account for the air mass of the template observation, a global aperture correction (mostly seeing dependent), and also the possible presence of clouds during the template observation (nonphotometric conditions). The color coefficients in the blue and red are $a1$ and $b1$, respectively. They correct for the color response of each Loral CCD at an air mass of zero. The color air-mass coefficients (0.022 and 0.004) are applicable to all stars. The chunk offset is a psuedoaperture correction relative to the centralmost corner chunk on a given CCD. It is unique for every field and chunk.

Calibrating MACHO instrumental photometry requires (1) field and (2) red west of pier chunk. For any object in the database, the field is known. It is the first number in the standard three-integer MACHO database identification number (*field.tile.sequence*). The red west of pier chunk is also known, but is not explicit in the identification number. The field number yields the style template (the layout of the focal plane), and the air masses of the template observations. The red west of pier chunk specifies location in the focal plane, which then uniquely specifies the zero points, color coefficients, template air mass, and chunk offset.

3.2. CTIO Observations

Observations were obtained in two week-long runs on the Cerro Tololo Inter-American Observatory (CTIO) 0.9 m telescope in December of 1994 and 1995 for the purpose of calibrating the MACHO database. We used the standard Tek 2048 × 2048 CCD and *BVRI* filter set to

[20] In the LMC top 22 fields, 8,468,104 out of 9,012,240 stars (actually objects) have two-color photometry.

make three or four observations of the center of each MACHO field using both V and R filters. Observations of each field were obtained at a wide range of air masses and on a minimum of three different nights. The LMC top 22 fields were given priority for observing when conditions were believed to be photometric. Typically, we observed 50 secondary standard stars of Landolt (1992) and Graham (1982) each night at several air masses. The secondary standards spanned a range of magnitudes and colors: $V \sim 12$–18 mag, and $V-R \approx -0.1$ to 1.2 mag. All photometry was performed with ALLSTAR II and DAOPHOT II (Stetson 1987, 1990). Transformation solutions for the CTIO instrumental photometry to the Kron-Cousins standard system were derived for each night using the Landolt and Graham standard-star observations. We employed a zero-point, color, and mean air-mass coefficient (for each week-long run) in the solutions. Residuals of these solutions showed typical standard deviations of 2%–3%, and 4% on the worst night. The zero points derived for the nightly transformation solutions varied significantly when the air-mass and color coefficients were fixed to run-averaged values, possibly indicating that the nightly average transparency had changed.

In some cases, the CTIO photometry (after applying the nightly transformations to V and R and aperture corrections) showed $\sim 10\%$ zero-point variations from night to night, which may indicate that some of our observations were obtained in nonphotometric conditions. However, our aperture corrections may also contribute to these apparent zero-point variations. The large number of images with very few bright and isolated stars lead us to calculate aperture corrections in the following manner. First, neighbors were subtracted from around several hundred of the brightest stars distributed evenly across each images. For each of these stars, standard curves of growth and statistics characterizing each curve were calculated. After some experimentation, we opted to calculate a single-valued aperture correction for each observation, ignoring any possible CCD position dependence. In some cases, poor subtraction of the neighbors leads to misestimates of the sky and thus inaccurate aperture corrections. In order to compensate for this effect, we adopted a rather small aperture (radius = 6 pixels = 2.″4) as a measure of the total flux, which was selected after careful examination of the Landolt and Graham standard-star observations.

Some repeat observations of the same fields on the same night suggested photometric conditions. Offsets were calculated to shift the nonphotometric CTIO photometry to these nights, and the photometry was averaged. Some of the averaged and single observation CTIO photometry were compared, and no significant or systematic changes in the colors were found. It is unlikely that the MACHO calibration color coefficients (or relative zero points) were affected by this choice to average the CTIO photometry. In some cases, the averaging appeared to yield tighter sequences in the CMDs. However, the averaging did not improve the precision of the derived calibration coefficients. We required that each star was detected in all CTIO observations for each field, which yielded approximately 100,000 calibration stars in our final lists.

3.3. Comparison of CTIO and MACHO Photometry

The CTIO tertiary standards are located at the center of each of the LMC top 22 fields. The field of view on CTIO 0.9 m telescope with the Tek CCD approximately covers the four central-most chunks of a MACHO field and thus one chunk from each of the four Loral CCDs (i.e., red west of pier chunks 3, 19, 31, and 51; see Fig. 2). These chunks are designated the "zero-point chunks." MACHO template photometry without blue jitter corrections was assembled for the zero-point chunks. Template coordinates were transformed to a globally consistent orientation. The CTIO photometry lists for each field were split into four quadrants, and the coordinates were shifted and scaled to the MACHO zero-point chunk photometry lists. The star lists were then matched using the method of similar triangles (Groth 1986). Automated matching of the star lists was quite difficult owing to the crowded fields and general lack of very bright reference stars. In particularly difficult cases, the star lists were split again and the procedure was repeated on all possible combinations of sublists until a satisfactory coordinate transformation was found.

Once the matched photometry lists were assembled, we obtained solutions for a variety of different photometric transformations with standard multivariate minimization techniques. Specifically, we obtained trial solutions that included nonlinearity coefficients, quadratic color terms, and color air-mass terms. However, these CTIO data did not satisfactorily constrain the higher order coefficients or warrant such complex transformation solutions. In additional experiments, we used different magnitude cuts and eliminated stars based on their fit to a constant brightness 1 year MACHO instrumental light curve. In the final solutions, no stars were eliminated for their variability.

Our final (linear) regressions yielded 88 zero points and color coefficients. We then performed linear regressions of the color coefficients with the template air-mass data to derive the best-fit CCD color coefficients at an air mass of zero ($a1$ and $b1$) for the adopted color air-mass coefficients (0.022 and 0.004). The color air-mass coefficients were also indicated by these regressions, but were somewhat poorly constrained. Therefore, we fixed their values (see also § 6.2 of this paper) and then derived the $a1$ and $b1$ coefficients. The uncertainties in the derived values of the $a1$ and $b1$ coefficients are estimated to be ~ 0.005; these coefficients are listed in Table 2. The color coefficients for CCDs 0 and 7

TABLE 2

CALIBRATION COLOR COEFFICIENTS

Blue CCD No.	$a1$	Red CCD No.	$b1$
1.....	−0.1876	6	0.1868
2.....	−0.2065	5	0.1784
3.....	−0.2059	4	0.1784
0[a].....	−0.2059	7[a]	0.1784

[a] The color coefficients for CCDs 0 and 7 are adopted (median of the other three CCD coefficients).

are adopted. They are never used for LMC or SMC calibration, only for the bulge.

Once the color coefficients were determined and fixed, the CTIO data were used to derive a single zero point and three relative CCD offsets (for each color) for each of the LMC top 22 fields. Trials with different data subsets indicated a typical uncertainty for zero points and offsets of order ~ 0.03 mag. In Figure 3, we present a CMD showing the CTIO data used to calibrate four zero-point chunks in MACHO field 13. We also show the difference between the calibrated CTIO and MACHO magnitudes as a function of V and R. Approximately 600 stars are plotted for each zero-point chunk. This figure illustrates the typical magnitude and color range of the CTIO tertiary standard stars and the typical dispersion of these data about the derived zero points.

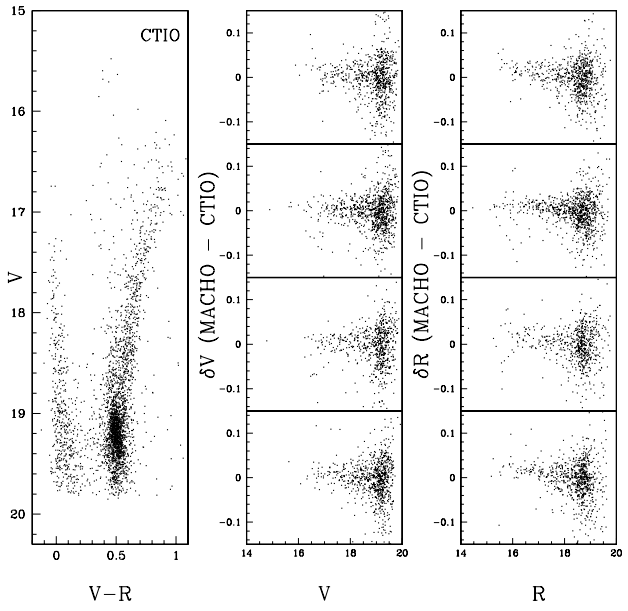


FIG. 3.—CTIO and MACHO calibration data for the four zero-point chunks in LMC field 13. The left panel shows the CTIO calibration data in the CMD; approximately 2500 stars are plotted. The difference in calibrated MACHO and CTIO photometry (δV and δR) as a function of V and R mag are plotted in the middle and right panels, respectively.

3.4. Chunk Offsets

Chunk offsets are aperture corrections relative to the zero-point chunk photometry for each CCD. The chunk offsets for the zero-point chunks are set equal to zero by definition. Using DAOPHOT, we obtained aperture photometry for several thousand bright stars in each MACHO template image. It was necessary to rereduce the template images with the appropriate flats and gain tables, as these have changed during the course of the experiment and the original reduced template images were not saved. It was assumed that the DAOPHOT aperture photometry, in a relative sense, uniformly measured the flux for these bright stars across the entire image. Coordinates of MACHO instrumental template photometry were transformed to the original image/pixel system, and stars were matched to the DAOPHOT aperture photometry lists. Chunk offsets were derived by comparison of the DAOPHOT aperture photometry with the SoDOPHOT template photometry.

Chunk offsets were derived for both the red and blue template images. Comparisons of photometry in field-overlap regions (see § 3.5) calibrated with the blue chunk offsets showed worse agreement than comparisons of photometry calibrated with no chunk offsets. Chunk offsets derived from the red image data and applied to both the red and blue photometry showed the best agreement in the field-overlap comparisons. The chunk offsets likely reflect the ability of the SoDOPHOT analytic PSF to fit the real instrumental PSF, which may change across the focal plane. In this case, the red image data appears to yield a more accurate measurement of the effect, for the technique we have used to calculate the chunk offsets. The chunk offsets are correlated with position in the focal plane, which is consistent with our explanation of their origin. In Figure 4, we plot the mean of the LMC top 22 field chunk offsets for each of the 64 chunks (red west of pier chunk number is in the lower right number of each box). The typical standard deviations for the mean chunk offsets are 0.02 mag.

3.5. Field-Overlap Comparison

Many of the MACHO fields in the LMC top 22 bar fields overlap the same region of sky.[21] The uncertainties of MACHO astrometry (typically an arcsecond) and the crowded nature of the bar fields complicates the identification of field-overlap stars. Probable pairs of field-overlap chunks were found via inspection of a map of our fields. Files of photometry with amplifier coordinates transformed to a globally consistent orientation were matched using the

[21] There is no complete census of field-overlap stars in the MACHO database, although it is estimated to be 6.5% of the total number of stars in the 22 bar fields. For a map of these fields, see Fig. 1 of Alcock et al. (1997).

0.029 124	0.022 120	0.028 4	0.017 0	0.013 15	−0.001 14	−0.010 13	−0.009 12
0.023 125	0.020 121	0.019 5	0.005 1	0.001 11	−0.004 10	−0.011 9	−0.010 8
0.014 126	0.011 122	0.008 6	−0.006 2	−0.003 23	−0.005 22	−0.007 21	−0.010 20
0.012 127	0.003 123	0.005 7	0.000 3	0.000 19	−0.004 18	−0.013 17	−0.015 16
0.023 48	0.012 49	0.009 50	0.000 51	0.000 31	−0.001 30	0.002 29	0.010 28
0.022 52	0.012 53	0.001 54	−0.008 55	−0.012 27	0.004 26	0.009 25	0.009 24
0.022 40	0.006 41	−0.005 42	−0.016 43	−0.020 39	0.002 38	0.011 37	0.012 36
0.036 44	0.017 45	0.002 46	−0.004 47	−0.009 35	0.006 34	0.007 33	0.014 32

FIG. 4.—Mean chunk offsets calculated for the top 22 field LMC calibration labeled on a chunk map to illustrate the focal-plane dependence. Listed in each of the 64 chunk locations is mean chunk offset (*upper left number*) and red west of pier chunk number (*lower right number*). See also Fig. 2.

method of similar triangles (Groth 1986). In this manner, approximately 360,000 stars in 150 chunk pairs were identified in field-overlap regions. These overlap regions allow us to check the precision of the photometric calibration for 21 of the top 22 LMC bar fields (field 47 is isolated). It was typical to measure the median offset between calibrated V and R magnitudes for two chunks in field-overlap regions with a precision of ~ 0.03 mag.

At this point in the calibration campaign, we attempted to globally minimize the zero points and offsets. This was a somewhat subjective procedure which required a high level of human interaction. We began with a handful of fields as calibration "anchor points" and then allowed the other fields' zero points to vary. Zero points were adjusted to minimize the offsets in field-overlap regions. In some cases, we also adjusted the CCD offsets (the zero-point offsets for the different CCDs relative to the single field zero point determined from the CTIO data). However, these were never changed by more than the estimated 1 σ uncertainty of their measured values (~ 0.03 mag). We additionally made a handful of "reality checks" (i.e., comparisons with published photometric standard sequences in our fields) throughout this global minimization procedure. Finally, the entire global minimization procedure was repeated several times. Each time we chose different anchor points and varied the sequential order of the field-by-field comparisons. In this manner, we endeavored to minimize possible systematic errors introduced by this procedure.

The MACHO photometry calibration described here yields an internal precision of $\sigma_V = 0.021$ *mag*, $\sigma_R = 0.019$ *mag, and* $\sigma_{V-R} = 0.028$ *mag* for ~ 9 million stars distributed over ~ 10 deg^2 of sky. This is illustrated in Figure 5 where we plot $\sim 20{,}000$ stars in 150 chunks with $V < 18$ mag. We plot the offset in V, R, and $V-R$ versus magnitude or color in the top, middle, and bottom panels, respectively. The standard deviations given above (and labeled in Fig. 5) are calculated from the median offsets determined for each of the 150 field-overlap chunk pairs.

4. COMPARISONS WITH OTHER PHOTOMETRY

4.1. Ground-based Data

It is customary to compare newly calibrated photometry with previously published data. We have arbitrarily selected ~ 200 stars representing photographic, photoelectric, and CCD data from a dozen different authors. This may be a representative sample. We restrict this comparison to our V photometry, because R photometry is less common. In § 4.2, we make comparisons with our V and R calibrated photometry, which allows the reader a more comprehensive assessment of the data.

We begin with a comparison of nine period-folded V-band light curves for an arbitrary sample of RR Lyrae and classical Cepheid variables. In Figure 6, from top to bottom then left to right we plot the classical Cepheids: HV 900, HV 905, HV 2510, HV 2352, and HV 2324, and the RR Lyrae variables near the cluster NGC 1835: GR 6, GR 14, GR 16, and Walker V26. The MACHO data consists of ~ 1000 measurements; they are plotted as dots. Error bars are omitted for clarity. The comparison data are plotted as filled circles and are assembled from Martin & Warren (1979: HV 900, HV 2323, HV 2352), Sebo & Wood (1995: HV 905), Martin (1981: HV 2510) and from Walker (1993: the RR Lyrae variable). For the RR Lyrae stars, the finding charts from Graham & Ruiz (1974) were also employed. We note that the photometry of Moffett et al. (1998; not plotted) for HV 900 also shows satisfactory agreement with the MACHO data. All of the RR Lyrae variables are located in the same MACHO field and chunk, thus the ~ 0.2 mag differences in brightness from star to star may not be attributed to a calibration error. These RR Lyrae variables illustrate the difficulty obtaining accurate photometry in crowded fields at this brightness.

In Figure 7, we compare our V photometry with various other data. We plot δV(MACHO − other) versus V mag. We designate different author's data with different symbols as follows. Asterisks are the Cepheid and RR Lyrae variables from Figure 6, filled circles are Walker's (1993) standard-star sequence near NGC 1835, open triangles are standard sequence of Cowley et al. (1990) near CAL 87 (finding chart found in Pakull et al. 1988), filled triangles are data from Flower (1982) near NGC 2058/2065, open squares are stars near NGC 1847 from Nelson & Hodge

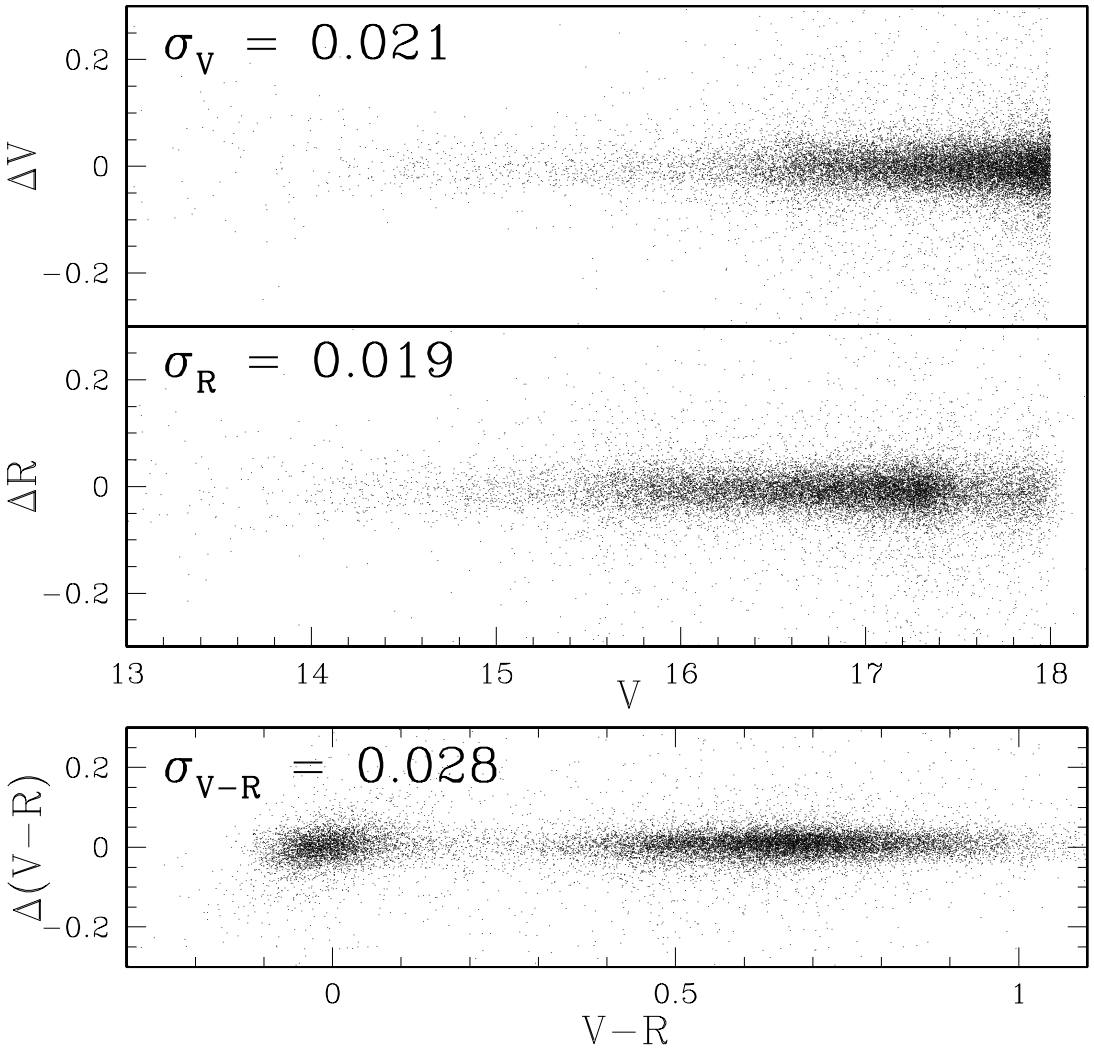


FIG. 5.—The differences in V, R, and $V-R$ for stars in field-overlap regions are plotted as a function of magnitude or color in the top, middle, and bottom panels, respectively. Approximately 20,000 stars are plotted; each has $V \lesssim 18$ mag and is located in 150 chunks tying together 21 of the LMC top 22 fields. The pairwise comparisons of overlapping chunk photometry are plotted in no particular order in a global sense, but all chunk pairs connecting the same two fields have been subtracted in the same order. Standard deviations, as described in the text and illustrated here, are labeled in each panel. These values indicate the precision of the calibrated MACHO photometry for ~ 9 million stars distributed over 10 deg^2 of the LMC bar.

(1983), and the open circles are photometry assembled from the classical LMC bar photometry paper by Tifft & Snell (1971). The median offset between MACHO and all of the other data is $\delta V = -0.035$ mag, which is indicated with a dashed line. Differences among the various authors likely represent systematic calibration errors.

4.2. *HST* Data

We have obtained *HST* Wide Field Planetary Camera 2 (WFPC2) image data with the F555W and F675W filters for three fields in the LMC top 22. These are located in the field-overlap region of MACHO fields 2 and 79, in field 13, and in field 11. The reader is referred to Alcock et al. (1997) for a map and sky coordinates of these fields. For each field, we obtained "shorts" (3–4 × 30 s exposures) and "longs" (3–4 × 400–500 s exposures), in both filters.

Complete details of the *HST* data reduction and analysis will be presented elsewhere (Nelson et al. 1999). Briefly, the images were co-added and geometrically corrected with the aid of the stand-alone Drizzle package (Fruchter & Hook 1998). We performed aperture photometry with the centroids accurately determined via PSF fitting using ALLSTAR II/ALLFRAME and DAOPHOT II (Stetson 1987, 1990). Stars were matched between filters for the longs and shorts separately and for each field observed. Only stars identified in both colors were kept in the final photometry lists. The median aperture correction was calculated from

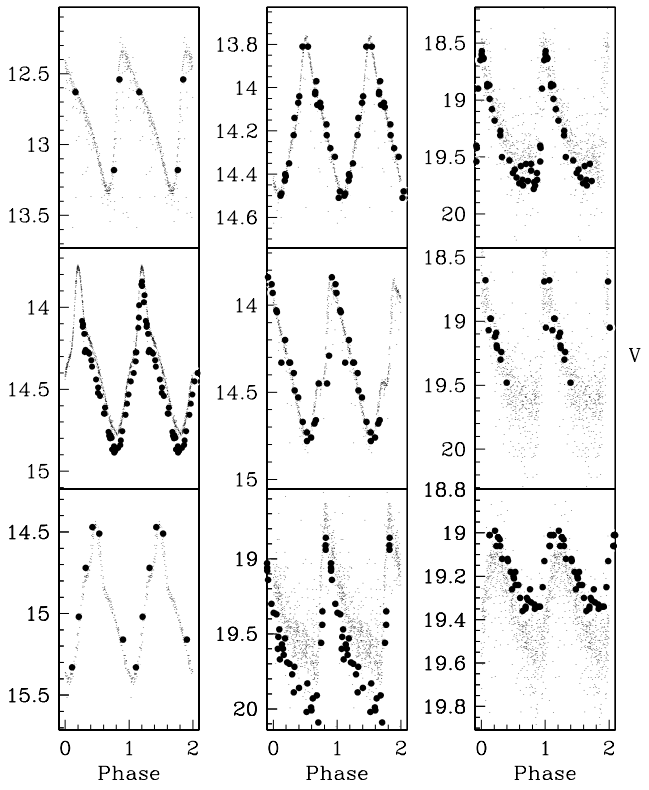


FIG. 6.—Period-folded MACHO V light curves compared with photometry data assembled from the literature (five different sources). MACHO data are plotted as dots and the comparison data as filled circles. Error bars are omitted for clarity. From top to bottom then left to right the variables are Cepheids: HV 900, HV 905, HV 2510, HV 2352, HV 2324, and RR Lyrae variables near the cluster NGC 1835: GR 6, GR 14, GR 16, and Walker V26. See text for further details.

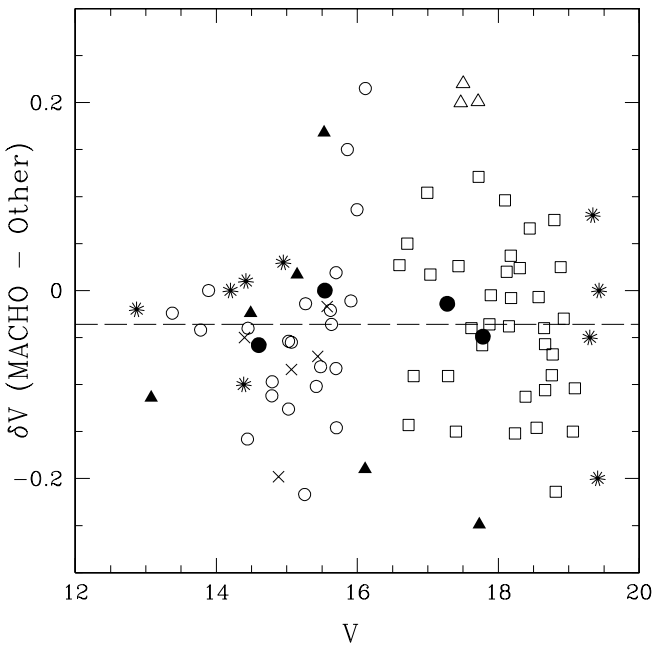


FIG. 7.—MACHO-calibrated V photometry in the LMC compared with various published measurements. The data are represented by the following symbols: asterisks are the Cepheids and RR Lyrae variables from Fig. 6, filled circles are Walker's (1993) standard-star sequence near NGC 1835, open triangles are standard sequence of Cowley et al. (1990) near CAL 87, filled triangles are data from Flower (1982) near NGC 2058/2065, open squares are stars near NGC 1847 from Nelson & Hodge (1983), and the open circles are photometry assembled from the classical LMC photometry paper by Tifft & Snell (1971). The median offset between the MACHO and all of the other data is indicated with a dashed line.

$\sim$50 bright and isolated stars per WF chip, per short or long exposure, and per filter. The photometry lists were calibrated according to Holtzman et al. (1995) using the coefficients in their Table 7 and the bay 4 gain ratios. The short and long photometry lists were then combined, including all stars found in either list, and adopting the long-exposure magnitudes for stars in common to both lists. We made no correction for the WFPC2 nonlinearity.

In Figures 8, 9, and 10 we compare approximately 120 stars identified in both the MACHO and *HST* photometry data. For each field we show the difference in magnitude, δV and δR (MACHO $-$ *HST*), as a function of V or R (*top two panels*) and $\delta(V-R)$ versus $V-R$ in the bottom panel. The open triangles are data from the WF2, the open circles are from WF3, and the open squares are from WF4. The median offset of the data is labeled in each panel. Typical dispersion about these median offsets is 0.02 mag. A direct comparison of ground-based and *HST* data is complicated by the radically different resolutions. We have simply added the flux for all *HST* stars inside a 1″ radius of the star identified as the match to the MACHO object. Various trials with different "artificial blending" schemes indicate that the precision of this comparison is $\sim$0.05 mag. It is difficult to identify the magnitude and angular separation (among pairs or groups of stars) where the faint *HST* stars "become sky" and would no longer be counted in the ground-based SoDOPHOT measurements. Resolution of this issue is beyond the scope of this work.

The MACHO and *HST* photometry comparisons in Figures 8–10 show agreement at the $\sim$5% level or better. We note that there are no systematic differences between the photometry derived for the three WF CCDs and the MACHO photometry (in each case, derived from a single CCD image), in three separate comparisons. Our fields are particularly useful for this comparison, because they are fairly uncrowded (for *HST*) and the comparison stars are distributed throughout each WF CCD, in each field. The apparent consistency of the calibrated WF photometry supports the procedure we have used for calculating the aperture corrections and also supports the calibration formulae for WFPC2 given by Holtzman et al. (1995). Given the $\sim$5% uncertainty associated with blending the *HST* data to match the MACHO data, these comparisons indicate that R agrees quite well, and that the calibrated colors are offset by 0.04 mag [i.e., $(V-R)_{HST} \approx (V-R)_{\rm MACHO} + 0.04$].

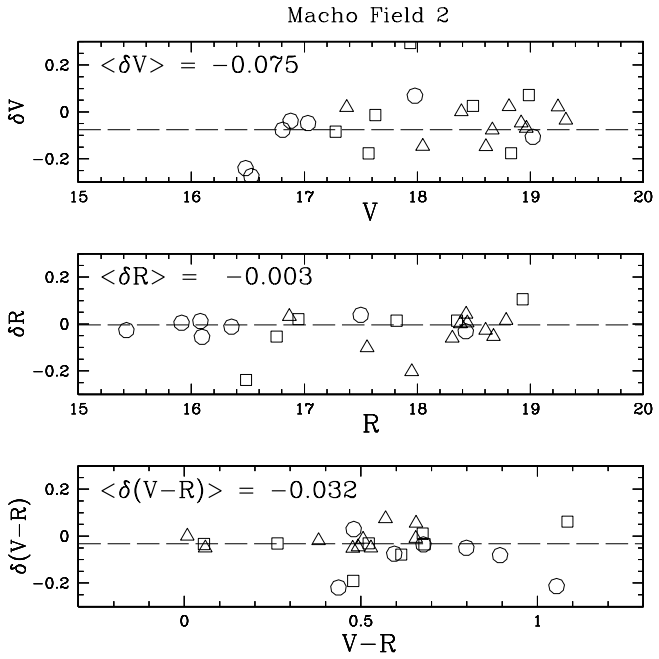


FIG. 8.—MACHO-calibrated photometry for field 2 compared with *HST*-calibrated photometry. Open triangles are data from the WF2 chip, open circles from WF3, and open squares from WF4. We plot the magnitude or color offset, δV, δR, and $\delta(V-R)$, in the sense (MACHO − *HST*) vs. magnitude or color. The median offset is labeled in each panel.

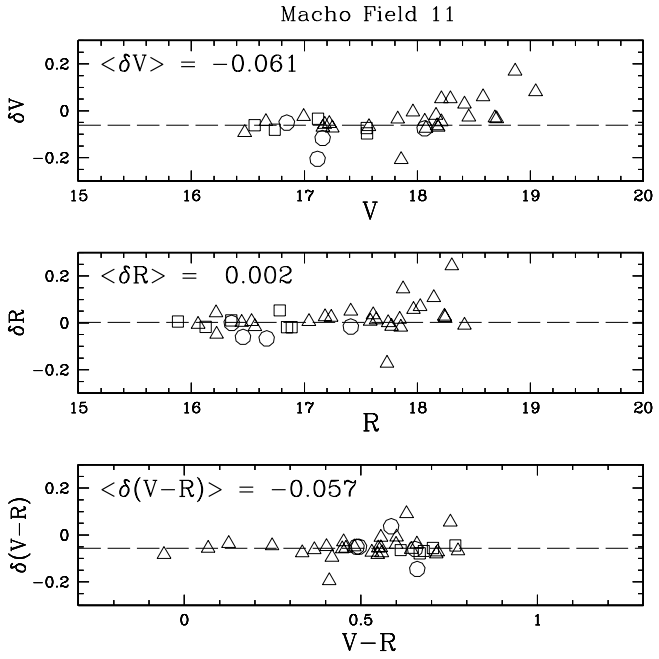


FIG. 9.—Same as Fig. 8, but for MACHO field 11

In Figure 11, we present two side-by-side CMDs showing the 120 MACHO objects and the "unblended" *HST* photometry from the comparison above. We plot the MACHO objects in the left panel and the *HST* stars in the right panel.

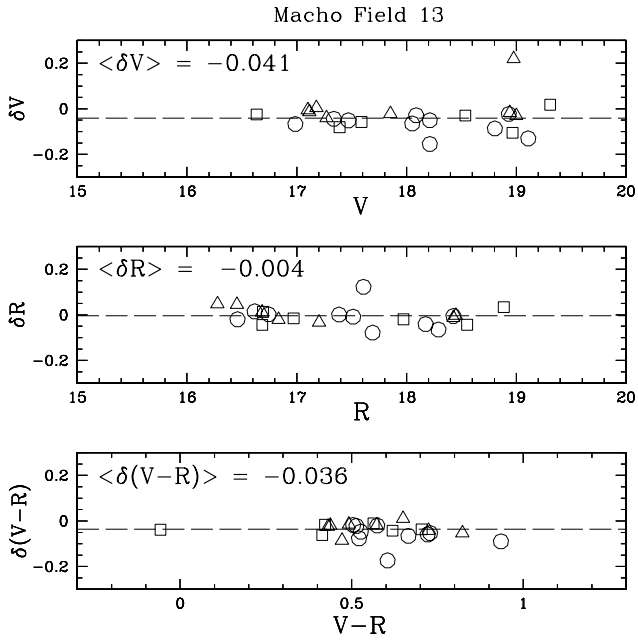


FIG. 10.—Same as Fig. 8, but for MACHO field 13

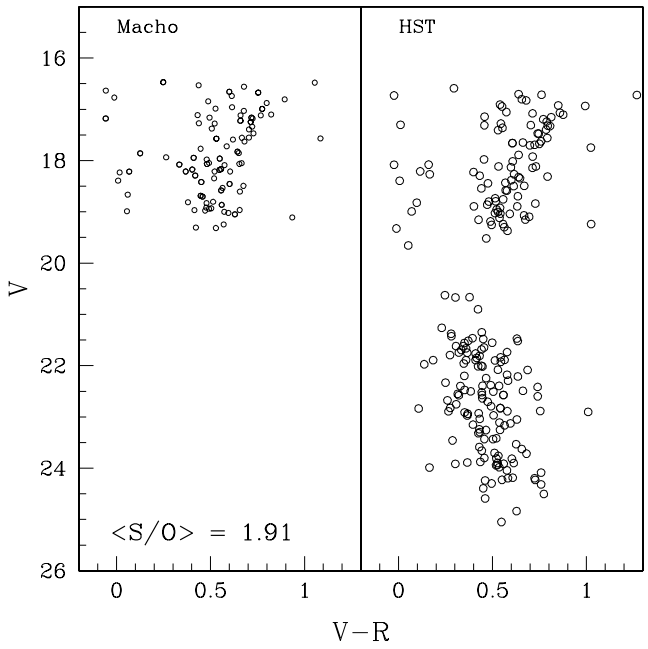


FIG. 11.—Color-magnitude diagrams showing the MACHO objects and (unblended) *HST* stars from Figs. 8–10. Each panel is labeled. The ratio of stars to objects is 229/120 = 1.91, also labeled.

Without making any corrections for completeness in the *HST* data, this naive comparison yields a star-to-object ratio S/O = 229/120 = 1.91. This value is sensitive to the adopted match radius (1″), but may reasonably be considered a lower limit to the average star-to-object ratio in these three fields. We will return to this in § 7.

5. OTHER MACHO FIELDS

5.1. Bulge Field 119 and SMC Field 207

We have calculated calibration zero points for field 119 (Baade's window) in the Galactic bulge and field 207 (near the cluster NGC 330) in the SMC by matching published photometry to MACHO data.

MACHO field 119 is centered on Baade's window. Calibrated photometry of ~ 70 stars from Cook (1986) and seven standard stars from Walker & Mack (1986) in the V and I passbands were converted to V and R using $V-R = 0.50(V-I)$ (e.g., Landolt 1992). These stars were then identified in the MACHO photometry database. The MACHO photometry was corrected for color and air mass according to equations (1) and (2) of this paper. Chunk offsets were assumed to be zero everywhere. In Figure 12, we plot the difference between the standard and color-corrected instrumental MACHO magnitudes as a function of V magnitude. The same plot is shown in the bottom panel for the R magnitudes. The median values of these magnitude differences are our adopted solutions for $a0$ and $b0$, and are plotted as solid lines in the top and bottom panels, respectively. The zero points are $a0 = 18.259$ and $b0 = 17.972$, with a standard deviation of ~ 0.025 mag.

The well-studied SMC cluster NGC 330 is located in MACHO field 207. We have used photometry from Vallenari, Ortolani, & Chiosi (1994) near NGC 330 to calibrate our SMC photometry. These data are in B and V, and we have converted them to V and R using $V-R = 0.56(B-V)$. The MACHO instrumental photometry was corrected for the color and air mass according to equations (1) and (2). We plot the data used for the field 207 zero-point solutions in Figure 13. We find $a0 = 17.788$ and $b0 = 17.584$, with a standard deviation of ~ 0.07 mag; these are indicated with solid lines in Figure 13.

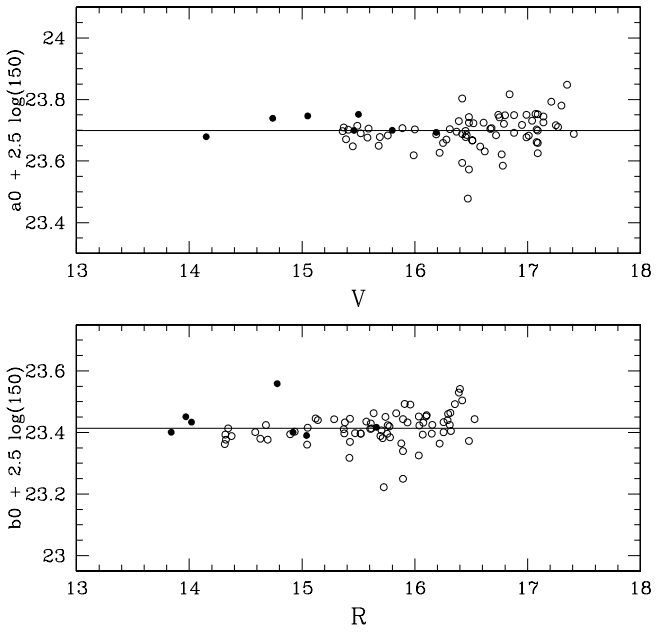


FIG. 12.—The solution for $a0$ and $b0$ using the published photometry of Cook (1986) and Walker & Mack (1990), plotted as open and filled circles, respectively, in MACHO bulge field 119.

5.2. Status of Calibration for All Other MACHO Fields

In Figure 14 we plot the LMC top 22 zero points ($a0$, *top panel*; $b0$, *middle panel*; and $a0 - b0$, *bottom panel*) as a function of template air mass (X_t) using small open circles. The single bulge zero point is plotted with a filled circle, and the single SMC zero point is plotted with a filled triangle. Linear regressions of the LMC top 22 zero-point data are indicated with dashed lines in each panel. We will use these to predict approximate zero points for all other MACHO fields in the LMC, SMC, and bulge. The derived regressions are

$$a0 = 18.410 - 0.279X_t\,, \tag{3}$$

$$b0 = 18.087 - 0.222X_t\,. \tag{4}$$

The uncertainty in the zero points are ± 0.06, and the uncertainty in the slopes are ± 0.04. The dispersion of the data about each of these regressions is ~ 0.10 mag. The data points lying below the regressions are likely due to non-photometric conditions (i.e., clouds), while the points above tend to have good seeing (this represents a by-field aperture correction, relative to the typical observation). At this time, the calibration zero-point uncertainty for all fields in the

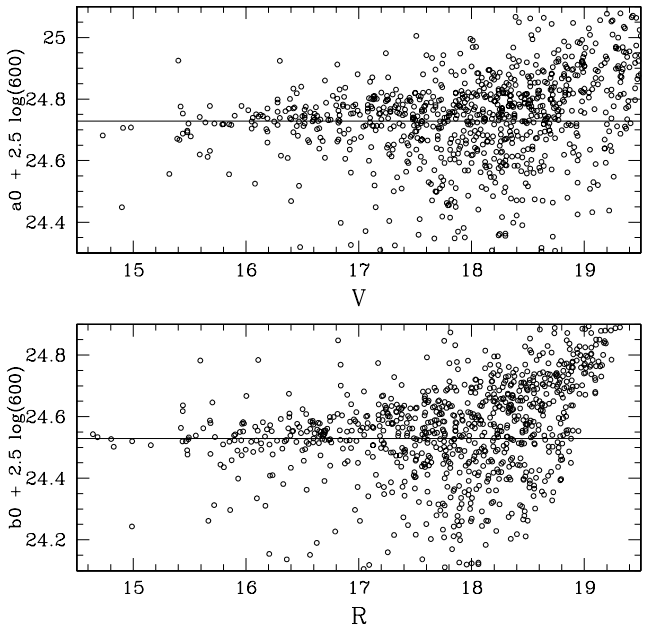


FIG. 13.—The solution for $a0$ and $b0$ using the published photometry of Vallenari et al. (1994) in MACHO SMC field 207.

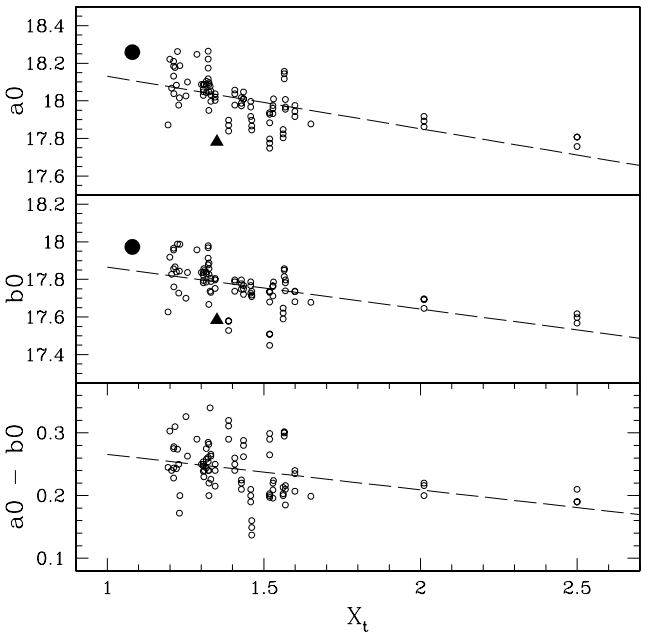


FIG. 14.—Calibration zero points ($a0$ and $b0$) for the top 22 LMC fields (*open circles*), Galactic bulge field 119 (*filled circle*), and SMC field 207 (*filled triangle*) plotted as a function of template air mass, X_t. Dashed lines show the regressions used to predict the calibrations zero points for all other MACHO fields.

MACHO database which have not been explicitly calibrated in this paper is 0.10 mag. The uncertainty in color is 0.04 mag, which is estimated from the dispersion about the $a0 - b0$ regression in the bottom panel of Figure 14.

6. LIGHT-CURVE CALIBRATION

6.1. Blue Jitter

MACHO instrumental light curves in the blue show a systematic source of scatter which is directly attributable to the responses of the different Loral CCDs and a secondary focal-plane position-dependent effect likely due to the dichroic. This is blue jitter. Because observations of LMC and SMC fields are made from both sides of the pier, stars will alternatively land on the CCDs rotated 180° from each other in the focal plane (i.e., a star will land in CCDs 4 and 6, or 5 and 7 depending on pier side). The opposite-pier side template photometry is modified (i.e., the template photometry is "jittered") so that PSF fitting in SoDOPHOT will converge quickly. This has the effect of *maintaining* the systematic differences in blue photometry derived from different pier side observations in the resulting instrumental light curves. It is possible to "de-jitter" light curves by applying the inverse of the template photometry blue jitter correction. The de-jitter algorithms have the form

$$V_{M,t} = V_{M,e} + \mathrm{BJ}_e[(V_{M,e} - R_{M,e}) - \mathrm{BJ}_0] , \qquad (5)$$

$$V_{M,t} = V_{M,w} + \mathrm{BJ}_w[(V_{M,w} - R_{M,w}) - \mathrm{BJ}_0] , \qquad (6)$$

where the subscripts "e" and "w" stand for east and west, respectively. The subscript "t" stands for template magnitude; thus $V_{M,t}$ calculated from equations (5) and (6) is an appropriate magnitude for input into equations (1) and (2). De-jitter corrections require an instrumental color for each measurement. They also require the three coefficients BJ_e, BJ_w, and BJ_0.

The coefficients BJ_e and BJ_w depend on (red west of pier) chunk and field. The field gives the style template, and the chunk specifies location in the focal plane. The coefficients BJ_e and BJ_w are unique for each chunk and applicable to all fields. However, the sign of the coefficient flips depending on the style template, and for every chunk, either BJ_e or BJ_w is set equal to zero. The BJ_w coefficients in Figure 15 are for blue jitter corrections in the imaginary case of a west of pier observation made of a field with template photometry derived from an entirely east of pier observation. This illustrates the focal-plane dependence.

The coefficient BJ_0 is unique to every field and chunk and is calculated from the mean color of the PSF stars in that chunk. BJ_0 is simply the color in each chunk where no blue jitter correction is necessary.[22] The calibration between BJ_0 and the mean color of the PSF stars in a chunk was derived

−0.007 124	−0.004 120	0.003 4	0.010 0	0.023 15	0.028 14	0.032 13	0.037 12
−0.012 125	−0.007 121	−0.000 5	0.004 1	0.017 11	0.022 10	0.026 9	0.032 8
−0.016 126	−0.013 122	−0.008 6	−0.001 2	0.013 23	0.018 22	0.020 21	0.024 20
−0.020 127	−0.016 123	−0.013 7	−0.008 3	0.008 19	0.012 18	0.014 17	0.018 16
−0.050 48	−0.046 49	−0.043 50	−0.040 51	−0.025 31	−0.020 30	−0.016 29	−0.010 28
−0.057 52	−0.053 53	−0.051 54	−0.047 55	−0.030 27	−0.024 26	−0.020 25	−0.016 24
−0.063 40	−0.061 41	−0.056 42	−0.052 43	−0.034 39	−0.028 38	−0.025 37	−0.022 36
−0.070 44	−0.066 45	−0.062 46	−0.055 47	−0.038 35	−0.032 34	−0.028 33	−0.026 32

FIG. 15.—Blue jitter BJ_w coefficients labeled on a chunk map to illustrate the focal plane dependence. Center in each of the 64 chunk locations is BJ_w while the red west of pier chunk number is the lower right number (see also Fig. 2). These coefficients are for blue jitter corrections in the imaginary case of a west of pier observation made of a field with template photometry derived from an entirely east of pier observation.

[22] The de-jitter correction applied to light curves for the 1 year and 2 year LMC microlensing analyses may be approximately recovered by setting BJ_0 equal to zero everywhere.

by minimizing the difference of mean blue magnitudes calculated using only east and west of pier data in the four-year light curves of ~400 constant brightness stars (per chunk), for 224 different chunks in 5 different LMC fields (9, 10, 18, 19, 82). These data are shown in Figure 16 along with our adopted calibration (shown as a solid line), which follows: for mean PSF colors $(V-R)_{\overline{\rm PSF}} < 0.35$ mag the coefficient $\rm BJ_0 = -0.05$ and for $(V-R)_{\overline{\rm PSF}} > 0.35$ mag the coefficient $\rm BJ_0 = -0.4 + (V-R)_{\overline{\rm PSF}}$. We estimate that de-jittering will be accurate to ± 0.02 mag with this procedure. The mean color of the PSF stars has been calculated for every chunk in the MACHO database.

6.2. Color Air Mass

MACHO instrumental light curves may show systematic changes in brightness which are correlated with the air mass of individual observations. Because of the limited observing season and the high priority set for observing the LMC, these fields are observed at progressively higher air masses as the season progresses. This may result in slow "seasonal rolls" (~1 year periods) in some instrumental light curves. We present here an algorithm for an air-mass and color-dependent light-curve correction. This correction is *not implemented* in any existing MACHO calibration code, but may potentially be useful for correcting small numbers of astrophysically interesting light curves.

The color air-mass corrections should be made on east and west of pier light-curve data separately before making blue jitter corrections. We show the form of the correction for east of pier data, maintaining the use of the subscript "e" to designate these measurements. The correction is equally applicable to the west of pier data. We designate the *raw* magnitudes with a prime. The color air-mass–corrected data does not have the prime and would be appropriate for substitution into equations (5) and (6) for blue jitter corrections. The color air-mass corrections have the form

$$V_{M,e} = V'_{M,e} + 0.033(X - X_t)[(V'_{M,e} - R'_{M,e}) - \mathrm{CA}_0] \,, \tag{7}$$

$$R_{M,e} = R'_{M,e} + 0.006(X - X_t)[(V'_{M,e} - R'_{M,e}) - \mathrm{CA}_0] \,, \tag{8}$$

where X is the air mass of each observation, X_t is the air mass of the template observation, and $\rm CA_0$ is the color for which no air-mass–correlated changes in brightness are observed. The ratio of the color air-mass coefficients in equations (1) and (2) to the color air-mass coefficients given in equations (7) and (8) are V: 0.022/0.033 and R: 0.004/0.006. Both ratios are ~0.66, which is approximately $(V-R)/(V_M-R_M)$. These color air-mass coefficients are derived from MACHO instrumental light curves, and support the values used in the calibration formulae, i.e., equations (1) and (2).

The $\rm CA_0$ coefficient varies from chunk to chunk, although no correlation was found with the mean color of the PSF stars, as was the case for the blue jitter $\rm BJ_0$ coefficient. Therefore, in order to make the color air-mass light-curve correction, $\rm CA_0$ must be derived using separate knowledge of the shape of a light curve. For example, one could solve for $\rm CA_0$ by minimizing the scatter in the period-folded light curve of a Cepheid variable star. An alternative way to solve for $\rm CA_0$ would be to minimize the scatter in several constant brightness stars in the same chunk as the star of interest. In this case, it is recommended that several nearby stars are used in the solution and that they have a wide range in colors, ideally bracketing the color of the star of interest. It is recommended to inspect scatter plots of $V_{M,e}$-X and $V_{M,w}$-X (separately, as blue jitter may mask the effect) in order to estimate the degree to which any particular light curve is affected.

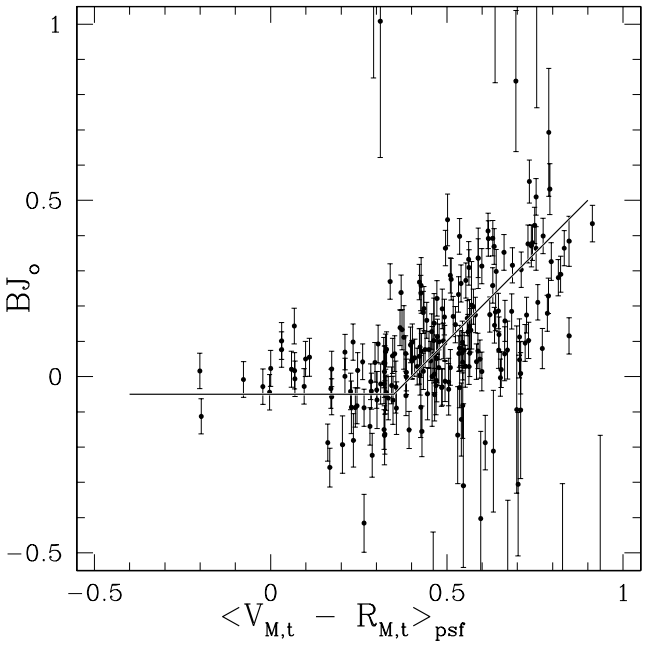


FIG. 16.—Data for 224 chunks in five different LMC fields used to derive the $\rm BJ_0$ – (mean color of PSF stars) calibration for the blue jitter corrections. The solid line is the adopted calibration.

6.3. Other Systematic Light-Curve Effects

We offer a few cautionary remarks to potential users of MACHO data. (1) Weather permitting, the MACHO Project will observe every night of the year. This includes nights when the seeing (the FWHM of the stellar PSF) approaches ~7″. In our typically crowded fields, poor seeing can lead to inaccurate photometry, despite the small photometric uncertainties that may be reported by

SoDOPHOT. Inspection of scatter plots of $V_{M,w}$-seeing and $V_{M,e}$-seeing are useful diagnostics for this source of systematic light-curve scatter. This so-called seeing variability can be quite large (easily a few tenths of a magnitude), particularly for very crowded stars or stars nearby regions of irregular, bright nebulosity. It is not recommended to globally decorrelate light curves with seeing. (2) The catalogs of CCD defects polluting the MACHO focal plane are not perfect. Uncataloged CCD defects will cause spurious photometric measurements, which are not necessarily reflected in the photometric uncertainty or integer flags reported by SoDOPHOT. In this case, inspection of the image data is very useful. (3) In some cases, light curves will exhibit additional scatter over that expected from the uncertainties of individual measurements which is not attributable to any of the aforementioned effects. This may be due to the inclusion of variable stars in the PSF fiducial lists used by SoDOPHOT. In this case, other light curves in the same chunk may also be affected.

7. THE EFFICIENCY CMD

The efficiency calculation will be reported in complete detail elsewhere (Alcock et al. 1999). Briefly, the calculation is a massive series of artificial star tests with raw image data spanning 4 years of observations followed by Monte Carlo experiments to detect fake microlensing events in accurately simulated artificial data sets. The efficiency calculation returns our sensitivity to detect microlensing in stars (not "objects"; see § 1). We calculate the star-to-object ratio in the MACHO data by comparing with the *HST* data. We assume that there are no objects in the high-resolution image data from the *HST*, only real stars.[23]

The efficiency CMD represents real LMC stars and contains accurate information on their surface density as a function of color and magnitude. For convenience, we use an area normalization of 0.52 deg^2 (one MACHO field). The limiting magnitude of the efficiency CMD is set by the faintest LMC star for which we may realistically detect microlensing. We adopt $V = 25$ mag, indicated by preliminary results from the efficiency Monte Carlo experiments. The efficiency CMD plays two roles in the efficiency calculation: (1) it is used to seed the artificial star tests with stars drawn from a realistic distribution in color and brightness, and (2) the derived efficiency (for stars) must be integrated over the efficiency CMD to calculate the efficiency per object in the MACHO database. The required accuracy of the efficiency CMD is dictated by the second application. The efficiency CMD has direct consequences for our measurement of the LMC microlensing optical depth.

[23] Observational data and further discussion of binary source stars (and lenses) will be presented in a forthcoming paper.

In Figure 17, we compare the three MACHO CMDs for fields 2, 11, and 13 for which we also have *HST* data (these are actually log-scaled Hess diagrams). Fields 2, 11, and 13 contain 354,586, 426,060, and 344,746 objects, respectively. We note that field 13 has the faintest limiting magnitude. Also, with the exception of the varying degree of differential reddening (field 11 is the most affected) and slight differences in the numbers of upper main-sequence stars, these three CMDs are quite similar.

In Figure 18, we compare the MACHO object luminosity functions with the *HST* star luminosity functions (LFs). We plot dN/dV as a function of V magnitude. The units of dN/dV are 10^4 stars (or objects) per 0.52 deg^2 in 0.125 V mag bins. The MACHO data are shown as solid lines. The *HST* data are shown as open circles connected by dotted lines. The typical error bar for the *HST* data is indicated in the upper right corner. We compare fields 2, 11, and 13 in the top, middle, and bottom panels, respectively. The *HST* data have been scaled to the MACHO data by a factor of 409, which is estimated as follows. The effective area photometered for each *HST* field is $3 \times 747.5 \times 747.5$ pixels. The plate scale of 0.″1 pixel^{-1} yields a sky area of 4.6 arcmin^2 per field. The MACHO plate scale of 0.″635 pixel^{-1}, and mosaic of $4 \times 2048 \times 2048$ Loral CCDs yields a total sky area of 1879.1 arcmin^2 per field. We scale the *HST* data by the ratio of sky areas after making a small (2%) correction for completeness in the *HST* data (see below). Figure 18 shows that the MACHO photometry is incomplete at the brightness of the red horizontal-branch clump ($V \sim 19.3$ mag) in fields 2 and 11. In contrast, field 13 appears complete to $V \sim 21$ mag.

In Figure 19, we compare the *HST* LFs for the three fields. We plot the logarithm of dN/dV (same units as in Fig. 18) as a function of V magnitude. Fields 2, 11, and 13 are shown as dotted, short-dashed, and long-dashed lines, respectively. The sum of these three LFs is shown as a bold line. Preliminary artificial star tests indicate that we are $\sim$98% complete to $V \sim 22$ mag. We have fitted a power law to the summed LF in the magnitude range $V = 19.5$–22 mag and extended it to $V = 25$ mag (the slope of the derived power law is $\alpha = 0.415 \pm 0.017$). The power-law LF is shown as a solid line. We assume this closely approximates the true LF. Deviations from the power-law fit may be due to incompleteness in the *HST* data or reflect a real turnover. We will use (below) the ratio the power-law LF to the summed *HST* LF to rescale the number of stars in the efficiency CMD from $V = 22$ to 25 mag. Considering only stars with $V < 25$, the summed *HST* LF contains 17,006,732 stars. The summed *HST* LF for $V < 22$ plus the power-law LF for $22 < V < 25$ contains 55,864,940 stars.

In order to improve the sampling of the sparsely populated bright end of the efficiency CMD, we will "splice" the bright MACHO data to the faint *HST* data. We will make the splice at $V = 18.7$ mag, where brighter than this, all

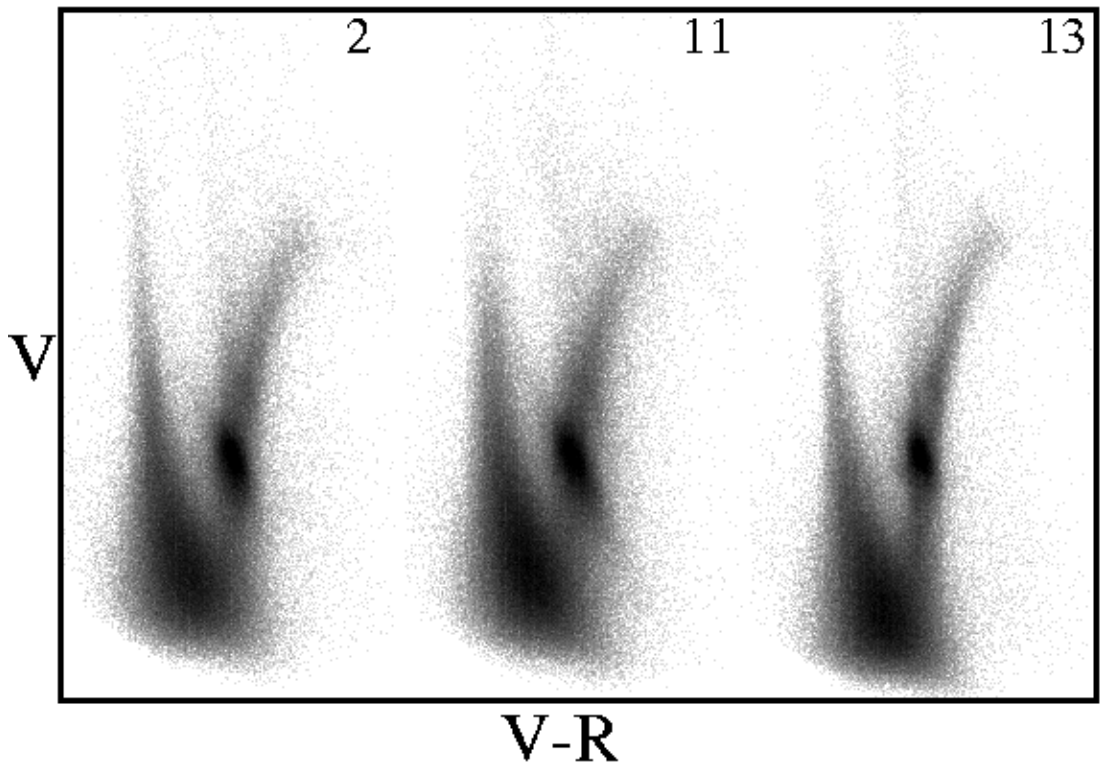


FIG. 17.—MACHO-calibrated Hess diagrams for LMC fields 2, 11, and 13. Although axes are not labeled, for each field they run from $V-R=-0.5$ to 1.5 mag (bin size 0.01 mag), and $V=22$ to 14 (bin size 0.02). Intensity represents the number of stars. The diagrams have been log scaled. These diagrams allow a qualitative comparison of the CMDs for each field.

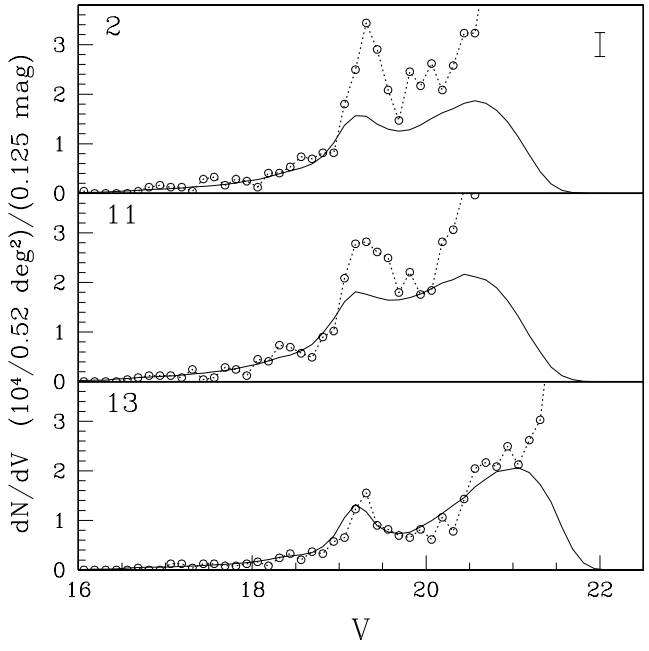


FIG. 18.—Luminosity functions for LMC fields 2, 11, and 13 comparing MACHO and *HST* data. The *HST* data has been scaled to the MACHO data. The typical error bar associated with each bin of *HST* data is indicated in the upper right corner.

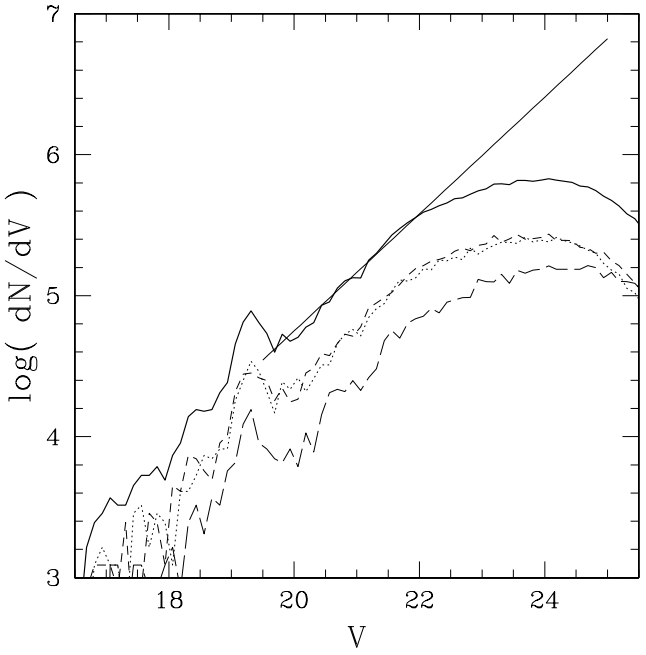


FIG. 19.—Luminosity functions for LMC fields 2, 11, and 13 comparing *HST* data. The units of dN/dV are as in Fig. 18. The sum of the three *HST* LFs is a bold line. Power-law fit and extension is solid line (see text).

three MACHO fields appear to be complete (see Fig. 18). The *HST* data and the MACHO data for the three fields are each binned in color from $V-R=-0.5$ to 1.5 in bins of 0.05 mag and in brightness from $V=25$ to 15 in bins of 0.10 mag. These two-dimensional histogram data are converted to images compatible with IRAF.[24] Within IRAF, we replace all pixels fainter than $V=18.7$ mag in the MACHO CMD image with zero values and similarly edit the *HST* image pixels values brighter $V=18.7$ mag. We additionally replace low-density pixels with zero values in each image. This step typically "removes" the few pixels containing galaxies, foreground stars, or bad measurements. In the *HST* image, these pixels would otherwise be scaled to very high values in the efficiency CMD. In the MACHO image, this step also removes features such as the upper main sequence, asymptotic giant branches, supergiants, and foreground Galactic disk stars. The regions of the CMD populated by these features are excluded in the searches for microlensing anyway. This editing has a negligible effect on total number of stars in the efficiency CMD.

Next, we sum the edited *HST* and MACHO images and smooth the resulting image. We multiply the spliced and smoothed CMD image by a power-law scaling image. The resulting efficiency CMD is shown in Figure 20. Intensity represents the number of stars. The image is log scaled; contours indicate 1.0, 3.5, 4.0, 4.5, 5.0, and 5.5 dex. The total number of stars represented is 55,426,384 (per 0.52 deg^2). The corresponding number of MACHO objects is 1,125,392, which yields a star-to-object ratio S/O = 49.2 to $V=25$. We find S/O = 1.2, 3.4, and 21.8 to $V=20$, 22, and 24 mag, respectively. These values are systematically uncertain at the $\sim$8% level, depending on the counting of MACHO objects identified only in one color.

It may be possible to adopt a single efficiency CMD for the entire LMC and then use the efficiency Monte Carlo experiments to sort out our relative sensitivities to detecting microlensing in different fields. However, we may also assess the uncertainty associated with the single efficiency CMD approximation as follows. Consider the three *HST* LFs in Figure 19. While the overall distributions are quite similar, fields 2, 11, and 13 contain 1,335,794, 1,406,142, and 595,913 stars (scaled to 0.52 deg^2) with $V<22$ mag. Using the total number of MACHO objects in these fields, we find S/O = 3.8, 3.3, and 1.7 for fields 2, 11, and 13, respectively, which yields $\langle S/O\rangle = 2.9 \pm 1.0$. The standard deviation indicates the uncertainty of our single efficiency CMD approximation. Because of the power-law LF correction for $V>22$ mag, the S/O to all fainter magnitudes scales directly from the $V\sim 21$ mag portion of the *HST* LFs.

We may extend this analysis to other fields using surface brightness measurements in the LMC. First, we measure

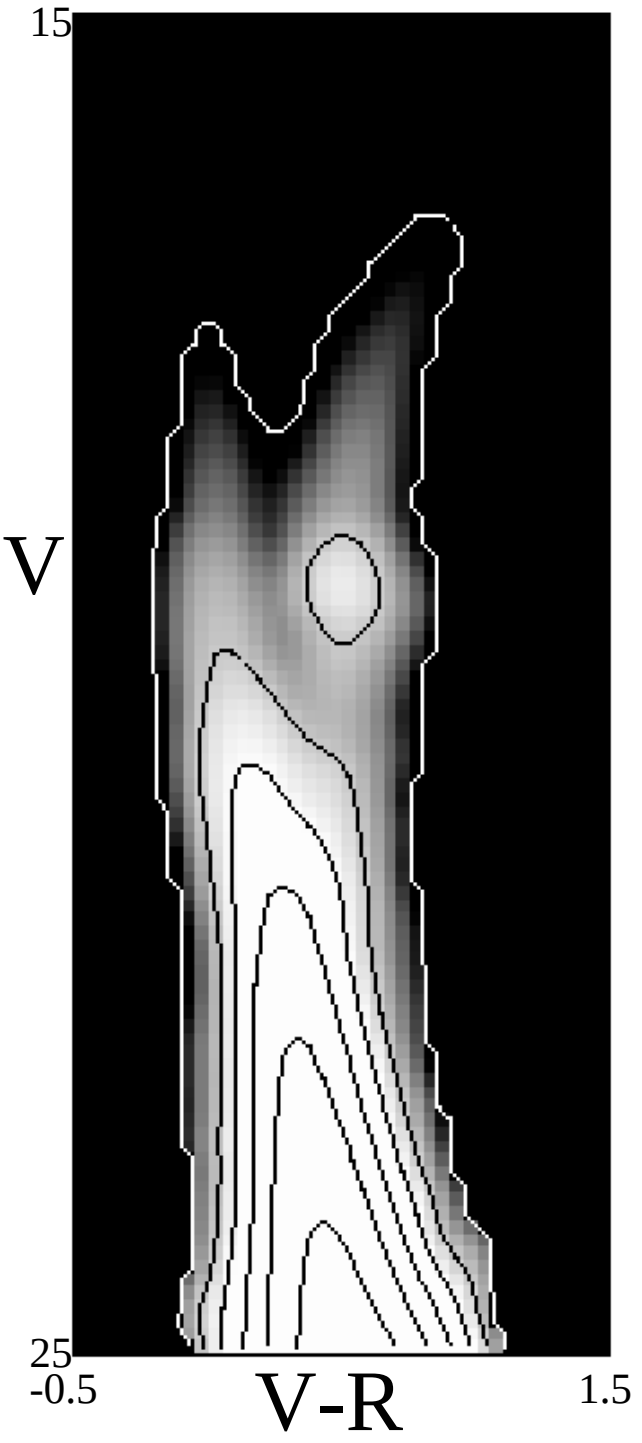


FIG. 20.—The efficiency CMD; a Hess diagram (two-dimensional histogram) representing the number of stars per 0.52 deg^2 in the LMC as a function of V and $V-R$. Intensity represents the number of stars. Logarithmic contours are overplotted in the diagram. The lowest contour (*white*) represents 1.0 dex stars [per $\Delta(V-R)=0.05$, $\Delta V=0.10$ mag bin, and 0.52 deg^2] while the other contours run from 3.5 to 5.5 dex in steps of 0.5 dex.

[24] The Image Reduction and Analysis Facility, v2.10.2, operated by the National Optical Astronomy Observatories.

relative fluxes (arbitrary units) for 16 MACHO fields from the Bothun & Thompson (1988) "Parking Lot Camera" wide-field *R*-band image of the LMC (the fields and this image are shown in Fig. 1 of Alcock et al. 1997). We exclude the centralmost bar fields because the image is saturated here. We also exclude two fields near 30 Doradus. The 16 fields selected span the "middle range" of the 30 fields targeted for the upcoming LMC microlensing analysis in terms of total number of objects. For our three fields with *HST* data, we perform a linear regression between the *HST*-derived S/O values and their surface brightnesses. We then use surface brightness to predict S/O for the remaining fields. These data are shown in Figure 21 where we plot S/O as a function of total number of objects per field (in units of 10^5 objects). Filled triangles are the S/O values calculated from the *HST* data for fields 2, 11, and 13. The filled circles are the fit values from the surface brightness regression for these three fields. The open circles are the estimates S/O values for the remaining fields. We are primarily concerned with the estimated scatter; the standard deviation is ~ 0.80, or a 30% uncertainty in S/O (also labeled on Fig. 21).

Figure 21 suggests a correlation between S/O and total number of MACHO objects per field. It may be the case that additional parameters (i.e., seeing or sky in the template images) would improve the correlation. If so, such a correlation may be used to rescale the efficiency CMD and improve the accuracy of the efficiency calculation, particularly as a function of position in the LMC. However, this analysis awaits further characterization of our SoDOPHOT-derived photometry and the efficiency Monte Carlo results.

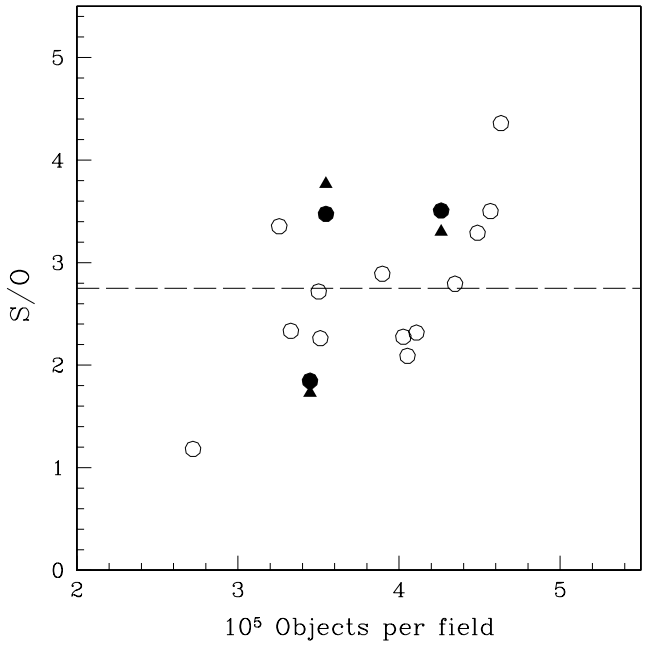


FIG. 21.—Star/object ratio (S/O) to the limiting magnitude $V = 22$ for 16 fields near the LMC bar as a function of the number of MACHO objects per field. Solid triangles are calculated from *HST*/MACHO photometry comparisons for three fields (see text). Solid circles show the fit values to a regression of these three S/O values and surface brightness measurements. The open circles show the S/O ratios predicted by the surface brightness regression for an additional 13 MACHO LMC fields.

8. SUMMARY

In this paper, we have described MACHO Project photometry data and calibration of these data. We have transformed our two-color instrumental photometry for ~ 9 million stars in the LMC top 22 fields (Alcock et al. 1997) to the Kron-Cousins *V* and *R* system with a precision of $\sigma_V = 0.021$, $\sigma_R = 0.019$, and $\sigma_{V-R} = 0.028$ mag. The uncertainties associated with the CTIO photometry aperture corrections and the MACHO transformation zero points are the most significant for the overall accuracy of the photometric calibration. We estimate ± 0.018 for the former and ± 0.03 mag for the latter, which is likely a correlated error in *V* and *R*. Therefore, we estimate the overall accuracy of these calibrated MACHO photometry to be ± 0.035 mag in *V*, *R*, and $V-R$. This appears consistent with comparisons of calibrated MACHO photometry data with published photometric sequences and calibrated *HST* observations. The accuracy of the calibrated MACHO photometry may be worse for stars with extreme colors owing to our nonstandard passbands. Calibration for all fields not including the LMC top 22 (Alcock et al. 1997), SMC field 207, and Galactic bulge field 119 has a zero-point uncertainty of 0.10 mag and a color uncertainty of 0.04 mag. The calibration presented in this work supersedes all prior calibration of MACHO photometry in the LMC, SMC, and Galactic bulge.

The detailed descriptions of the data reduction and photometry database provided in this work are largely intended to guide consumers of released MACHO data. If potential calibrators have assembled MACHO instrumental template photometry, or otherwise adopted/calculated MACHO instrumental magnitudes and colors as substitutes for the original template photometry, the necessary calibration formulae are given in § 3.1. We have additionally discussed the calibration of MACHO light curves. If potential calibrators will make detailed analyses of MACHO light curves, they should consider making corrections for known systematic effects such as blue jitter (§ 6.1), color-dependent air-mass variability (§ 6.2), as well as effects due to seeing and uncataloged focal-plane defects (§ 6.3). Last in this work, we have described the construction of the efficiency CMD, a cornerstone of the new microlensing detection efficiency calculation, which will be presented in a forthcoming MACHO collaboration paper.

David Alves thanks his graduate advisors, Kem Cook and Robert Becker, for their support. We thank the skilled

support by the technical staff at MSSSO. Work at LLNL supported by DOE contract W7405-ENG-48. Work at CfPA supported by NSF AST-8809616 and AST-9120005. Work at MSSSO supported by the Australian Department of Industry, Technology and Regional Development. W. J. S. thanks PPARC Advanced Fellowship; K. G. thanks DOE OJI, Sloan, and Cottrell awards; C. W. S. thanks Sloan and Seaver Foundations.

REFERENCES

Alcock, C., et al. (The MACHO Collaboration). 1997, ApJ, 486, 697
———. 1999, PASP, in press
Axelrod, T., et al. (The MACHO Collaboration). 1998, Proc. SPIE, 3349, 152
Bessell, M. S. 1979, PASP, 91, 589
———. 1986, PASP, 98, 1303
———. 1990, PASP, 102, 1181
———. 1995, PASP, 107, 672
Bessell, M. S., & Weis, E. W. 1987, PASP, 99, 642
Bothun, G. D., & Thompson, I. B. 1988, AJ, 96, 877
Cook, K. 1986, Ph.D. thesis, Univ. Arizona
Cowley, A. P., Schmidtke, P. C., Crampton, D., & Hutchings, J. B. 1990, ApJ, 350, 288
Flower, P. J. 1982, PASP, 94, 894
Fruchter, S., & Hook, R. 1998, in preparation (astro-ph/9808087)
Graham, J. A. 1982, PASP, 94, 244
Graham, J. A., & Ruiz, M. T. 1974, AJ, 79, 363
Groth, E. J. 1986, AJ, 91, 1244
Hart, J., et al. (The MACHO Collaboration). 1996, PASP, 108, 220
Holtzmann, J. A., Burrows, C. J., Casertano, S., Hester, J. J., Trauger, J. T., Watson, A. M., & Worthey, G. 1995, PASP, 107, 1065
Landolt, A. U. 1992, AJ, 104, 340
Marshall, S. 1994, Ph.D. thesis, Univ. California, Santa Barbara
Martin, W. L. 1981, South African Astron. Obs. Circ., 6, 96
Martin, W. L., & Warren, P. R. 1979, South African Astron. Obs. Circ., 1, 98
Moffett, T. J., Gieren, W. P., Barnes, T. G., & Gomez, M. 1998, ApJS, 117, 135
Nelson, C. A., et al. 1999, in preparation
Nelson, M., & Hodge, P. 1983, PASP, 95, 5
Paczýnski, B. 1986, ApJ, 304, 1
Pakull, M., Beuermann, K., van der Klis, M., & van Paradijs, J. 1988, A&A, 203, L27
Robinson, T., & Grubb, T. 1869, Philos. Trans. R. Soc., 159, 127
Schechter, P. L., Mateo, M., & Saha, A. 1993, PASP, 105, 1342
Sebo, K. M., & Wood, P. R. 1995, ApJ, 449, 164
Stetson, P. B. 1987, PASP, 99, 191
———. 1990, PASP, 102, 932
Stubbs, C., et al. (The MACHO Collaboration). 1993, Proc. SPIE, 1900, 192
Tifft, W. G., & Snell, C. M. 1971, MNRAS, 151, 365
Vallenari, A., Ortolani, S., & Chiosi, C. 1994, A&AS, 108, 571
Walker, A. R. 1993, AJ, 105, 527
Walker, A. R., & Mack, P. 1986, MNRAS, 220, 69